Traction Forces of Neutrophils Migrating on Compliant Substrates

Risat A. Jannat,[†] Micah Dembo,[§] and Daniel A. Hammer[†‡*]
[†]Department of Bioengineering and [‡]Department of Chemical and Biomolecular Engineering, University of Pennsylvania, Philadelphia, Pennsylvania; and [§]Department of Biomedical Engineering, Boston University, Boston, Massachusetts

ABSTRACT Proper functioning of the innate immune response depends on migration of circulating neutrophils into tissues at sites of infection and inflammation. Migration of highly motile, amoeboid cells such as neutrophils has significant physiological relevance, yet the traction forces that drive neutrophil motion in response to chemical cues are not well characterized. To better understand the relationship between chemotactic signals and the organization of forces in motile neutrophils, force measurements were made on hydrogel surfaces under well-defined chemotactic gradients created with a microfluidic device. Two parameters, the mean chemoattractant concentration (C_M) and the gradient magnitude ($\Delta c/\Delta x$) were varied. Cells experiencing a large gradient with C_M near the chemotactic receptor K_D displayed strong punctate centers of uropodial contractile force and strong directional motion on stiff (12 kPa) surfaces. Under conditions of ideal chemotaxis—cells in strong gradients with mean chemoattractant near the receptor K_D and on stiffer substrates—there is a correlation between the magnitude of force generation and directional motion as measured by the chemotactic index. However, on soft materials or under weaker chemotactic conditions, directional motion is uncorrelated with the magnitude of traction force. Inhibition of either β_2 integrins or Rho-associated kinase, a kinase downstream from RhoA, greatly reduced rearward traction forces and directional motion, although some vestigial lamellipodium-driven motility remained. In summary, neutrophils display a diverse repertoire of methods for organizing their internal machinery to generate directional motion.

INTRODUCTION

Relating observations of cell motion to underlying mechanical processes is a major aim in the field of cell migration. During migration, adherent cells generate traction forces at the cell-substrate interface that enable net displacement. Traction forces can vary significantly in magnitude, location, orientation, and timescale, depending on the cell type and its physiological function. In addition, chemical and mechanical conditions in the local microenvironment surrounding a cell can influence force generation. Initial studies of cellular forces focused on anchorage-dependent cells such as fibroblasts, endothelial cells, and epithelial cells and demonstrated that these cell types are capable of applying large traction forces on the order of 10,000 nN on their underlying substrates during adhesion and chemokinesis (1–7). Simultaneous imaging of traction forces and fluorescently tagged adhesion proteins within individual cells have shown that forces are associated with focal adhesions and that adhesions at the leading edge of the cell are the sites of active force generation and propulsion (8,9). A frontal towing model of motility has been proposed to explain the spatial and temporal distribution of traction forces at the leading edge in anchorage-dependent cells (9).

Although the process of cellular force generation in anchorage-dependent cells has been under intense investigation for more than three decades, force measurements of fast-moving cells such as keratocytes, *Dictyostelium*, metastatic tumor cells, and immune cells such as neutrophils have been elusive until recently (7,10–16). Studies of these cells types have revealed that the highest traction forces in highly motile cells are located at the rear of the cell relative to movement (12,13,16,17). Average forces in these high-speed cells are approximately two orders of magnitude lower than those observed for anchorage-dependent cells, as expected based on the previously established inverse correlation between speed and force (18). The presence of higher traction forces at the rear during motion suggests that rapidly-migrating amoeboid cells generate forward propulsion using a system of forces and molecular assemblies distinct from that of anchorage-dependent cells. To further assess the core mechanical principles that govern the motility of rapidly migrating cells, we examined the traction forces of neutrophils in response to chemoattractant signals.

Neutrophils are key players in the inflammatory response to injury and pathogens and their activation by chemoattractants leads to firm adhesion and migration (19). The response of neutrophils to chemoattractants during chemokinesis and chemotaxis has been studied extensively on stiff glass substrates and is well characterized (20). More recently, we and others have examined neutrophil chemokinesis and chemotaxis on hydrogel substrates (16,17). Under a linear gradient $\Delta c/\Delta x$ of chemoattractant c(x), where the mean concentration of chemoattractant is C_M at the cell center, neutrophils display increased directional migration with increasing $\Delta c/\Delta x$ and respond most effectively when C_M is near the K_D of chemotactic ligand binding for the receptor (18,22). Chemoattractant gradients rapidly induce neutrophil polarity and the formation of distinct pseudopodial and uropodial regions. In the presence of uniform

Submitted June 22, 2010, and accepted for publication May 3, 2011.

*Correspondence: hammer@seas.upenn.edu

Editor: Jason M. Haugh.

0006-3495/11/08/0575/10 $2.00

doi: 10.1016/j.bpj.2011.05.040

stimulation, morphologic polarity is also observed, although the cell will move in random directions (23). The formation of neutrophil polarity begins with chemoattractant receptor-activated G-proteins that initiate divergent signaling through Rho GTPases and the formation of spatially segregated frontness and backness signaling modules (24). At the leading edge, accumulation of Rac leads to F-actin polymerization and the extension of pseudopods. At the sides and rear, RhoA activity stimulates contractility through p160-ROCK and myosin II (25). To date, the spatial patterns of these molecules have not been correlated with the spatial pattern of traction stresses in these cells.

The rapid motility of neutrophils combined with their well-defined responses to chemical signals makes them an ideal system for investigating the relationship between signaling, motility, and force generation in amoeboid cells. Using traction force microscopy and microfluidic gradients, we measured neutrophil forces on compliant hydrogel substrates in uniform and gradient solutions of the chemoattractant fMLP (Fig. 1). In a previous study, we and others demonstrated that cellular forces depend on integrin adhesion and that integrin adhesion can trigger RhoA activity through force-dependent pathways (26). To examine how neutrophils generate traction forces on substrates with different mechanical properties, we examined the effect of inhibiting signals through $\beta 2$ integrins and RhoA. We found a direct correlation between chemotactic signal and the magnitude and polarity of traction stresses on stiff surfaces and under strong chemotactic signals. On stiffer materials, smaller values of the gradient, $\Delta c/\Delta x$, or changes in C_M away from the K_D of receptor binding led to less intense force generation, lower root-mean-squared forces, and a smaller chemotactic index. Under chemokinesis (in a uniform field of chemoattractant), cells exerted lower root-mean-squared forces and moved randomly. We also found that the substrate plays a role in controlling directional motion: stiffer substrates allow cells under the same chemoattractant gradient to organize more efficiently and generate larger traction stresses. On soft materials or weak chemoattractant signals, cells can display directional motion that is uncorrelated with traction stress. Our data provide insight into the coordination of neutrophil forces that is critical for understanding how these cells migrate through tissue compartments to hunt pathogens and respond to inflammation.

MATERIALS AND METHODS

Reagents

Adhesive ligands were Protein G (Pierce Biochemicals, Rockford, IL), human ICAM-1 Fc, and E-Selectin Fc (R&D Systems, Minneapolis, MN). TS1/18 $\beta 2$ integrin antibody was used at 10 μg/mL to block adhesion (Pierce Biochemicals) (27), neutrophils were activated with fMLP chemoattractant peptide (Sigma-Aldrich, St. Louis, MO), and cell contractility was inhibited using 10 μm Y-26732 ROCK inhibitor (Calbiochem, San Diego, CA).

Isolation of neutrophils

Whole blood was obtained from healthy human donors by venipuncture and collected in BD Vacutainer tubes containing citrate-EDTA anticoagulant (Becton Dickinson, Franklin Lakes, NJ). Blood was layered onto

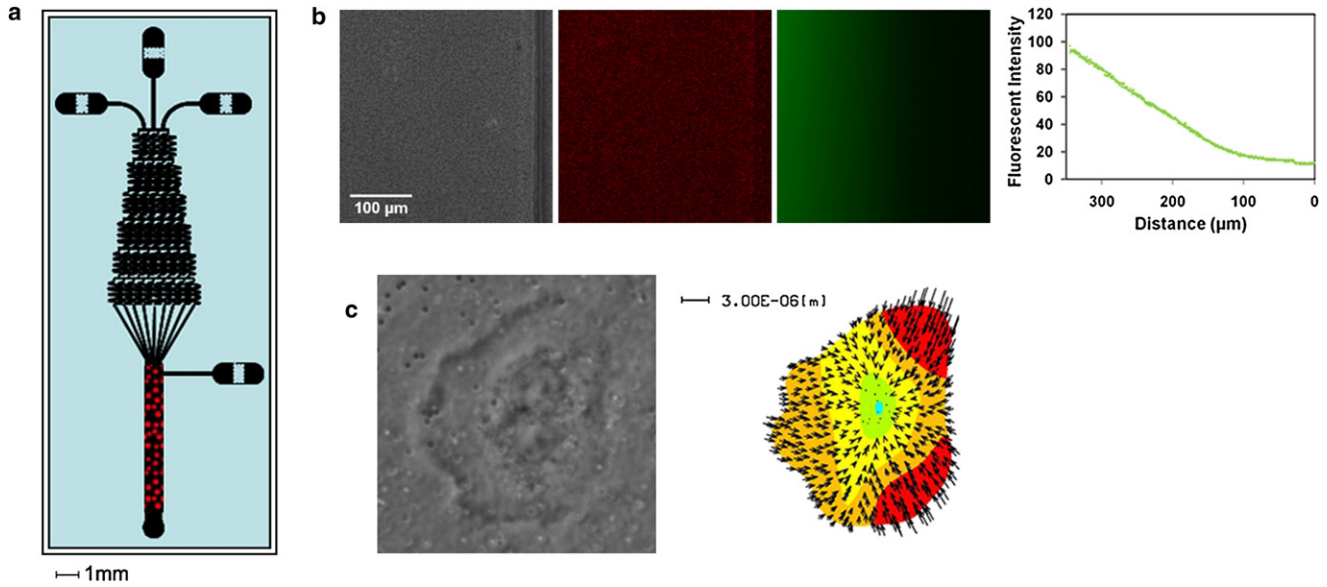

FIGURE 1 Overview of microfluidic traction force chamber. (*a*) A microfluidic gradient generator was used to create linear gradients over a traction force gel embedded in the main channel area of the device. Red dots represent the region where the traction force gels are placed and cells are observed. (*b*) Phase-contrast (*left*) and fluorescent-bead images (*middle*) of a traction force gel within the main channel of a microfluidic chamber, along with an image of fluorescein dye solution (*right*) flowing through the same region. At far right, an intensity plot of fluorescein fluorescence shows that a linear gradient is developed and maintained over the hydrogel. (*c*) Phase-contrast and traction-force microscopy map of a neutrophil oriented within the chamber in response to a chemical gradient.

Polymorphprep density gradient medium (Axis-Shield, Oslo, Norway) and centrifuged at 500 g for 1 h. After centrifugation, the neutrophil fraction was aspirated and washed once by centrifugation at 350 g for 10 min in Hanks' balanced salt solution without Ca^{2+} and Mg^{2+}. Washed neutrophils were then resuspended in Hanks' balanced salt solution without Ca^{2+} and Mg^{2+} that had been supplemented with 0.1% human serum (Sigma-Aldrich, St. Louis, MO) and 10 mM HEPES (Invitrogen, Carlsbad, CA). Before use in flow chamber assays, neutrophil solution was supplemented with 1.5 mM Ca^{2+} and 2.0 mM Mg^{2+}.

Preparation of hydrogel substrates

Polyacrylamide hydrogels were prepared as described previously by Pelham and Wang, with slight modifications (28). Briefly, Corning glass coverslips were silanized with 3-aminopropyl-trimethoxysilane (APTS) (Sigma-Aldrich, St. Louis, MO) and activated with 0.5% glutaraldehyde solution (Sigma-Aldrich). Acrylamide solutions were prepared that contained either 5% or 7% w/v of a 40% acrylamide stock solution (Bio-Rad, Hercules, CA), varying concentrations of N,N′-methylene-bis-acrylamide ranging from 0.1% to 0.76% (Bis, 2% w/v stock solution, Bio-Rad), 35 mM HEPES, pH 8, and distilled water. The concentration of Bis was varied to control the mechanical properties of the hydrogel. Higher concentrations of Bis result in a greater degree of gel cross-linking and an increase in shear modulus (G'). Gel stiffnesses were confirmed by mechanical testing using a Q800 Dynamic Mechanical Analysis instrument (TA Instruments, New Castle, DE) and were found to be ~2 kPa for soft gels and 12 kPa for stiff gels. To covalently link proteins to the surface of hydrogels and render them adhesive to cells, 6-((acryloyl)amino)hexanoic acid (N-6) cross-linker was synthesized according to the method of Pless et al. (29) and co-polymerized with acrylamide and Bis. Gel solutions containing 500 nm red fluorescent beads (Invitrogen) were degassed and photopolymerized onto activated glass coverslips using 0.5% w/v Irgacure 2959 photoinitiator (Ciba, Newport, DE) to produce thin hydrogels immobilized on glass coverslips. Gels were rinsed with ice cold distilled water and trimmed to dimensions compatible with the main channel area of the microfluidic flow chamber.

Fabrication and assembly of microfluidic flow chambers

Gradient-generating microfluidic networks were designed according to principles described by Dertinger and Whitesides (30). Microfluidic chambers used in this study were fabricated by bonding polydimethylsiloxane (PDMS) chambers (Sylgard 184, Dow Corning, Midland, MI) to glass coverslips containing hydrogels (31). PDMS chambers with gradient-generating channels were prepared from silicon wafer templates using standard photolithography techniques. SU8 photoresist film (MicroChem, Boston, MA) was patterned on the surface of a silicon wafer by exposure to UV light through a high-resolution negative transparency mask in a Karl Süss (Garching, Germany) mask aligner. After exposure, un-cross-linked regions of the film were developed away, leaving a raised network of channels on the surface of the wafer. PDMS chambers with embedded channels were prepared by pouring a 10:1 ratio of PDMS polymer to cross-linking agent onto the silicon template, degassing, and curing in an oven for 1 h at 80°C. Cured PDMS chambers were peeled away from wafer templates and trimmed down to the size of glass coverslips. Inlet and outlet ports were punched into the chamber using a blunt-end needle.

To permanently seal PDMS chambers to glass coverslips containing immobilized hydrogels, PDMS and glass surfaces were briefly exposed to reactive oxygen plasma under vacuum. The main channel of the microfluidic device was aligned with the hydrogel substrate, and the surfaces were pressed into contact. Hydrogels within assembled microfluidic devices were incubated with 0.5 mg/mL of Protein G diluted in 50 mM HEPES buffer, pH-6 at 4°C overnight. Unreacted N6 cross-linker on the surface of the hydrogel was capped by incubating with a 1:100 dilution of ethanolamine for 30 min at room temperature. Hydrogels were rinsed with 0.1 M sodium carbonate buffer, pH 9, and incubated with 50 μg/mL of ICAM-1 Fc and 50 μg/mL of E-Selectin Fc for 2 h at room temperature. Each assembled microfluidic device was used once.

Cell tracking and quantitation of motility

Positions of firmly adherent cells at different positions within a microfluidic chamber were captured using a Nikon Inverted Eclipse TE300 microscope with a Nikon 20×, numerical aperture 0.40 objective. Time-lapse images were recorded at 30- or 60-s intervals for a minimum of 10 min for migration experiments. The position of individual cell outlines at each time interval was recorded, and cell centroids were determined using ImageJ software. For each chemoattractant gradient, a mean time-averaged concentration (C_M) and slope ($\Delta c/\Delta x$) was calculated. In the presence of linear gradients, the chemotactic index was calculated by measuring the distance traveled in the direction of the gradient divided by the total path length. Data from individual cells was averaged to obtain a single value for each parameter and condition evaluated.

Traction force microscopy

Traction force microscopy was performed as described previously on firmly adherent cells within microfluidic chambers using a Nikon Inverted Eclipse TE300 microscope with a Nikon 100×, numerical aperture 1.30 oil objective (5,13). Phase contrast and corresponding fluorescent bead images were captured simultaneously for each cell at 1-min intervals. At the end of each experiment, cells were removed from the gel by addition of a trypsin-EDTA solution, and an image of the unstressed gel was taken. Traction forces were determined based on deformations of the hydrogel substrate as reported by the motion of fluorescent beads embedded within the top surface. Using custom-written LIBTRC 2.0 software, bead displacements within the area of cell contact were calculated and the most likely surface traction force vectors were obtained as described by Dembo and Wang (32). The average or root-mean-squared force ($|F|$) exerted by the cell on the substrate is an integral of the traction stress over the cell contact region, $|F| = \iint \sqrt{T_x^2(x,y) + T_y^2(x,y)}dxdy$, where $T(x,y) = [T_x(x,y),\ T_y(x,y)]$ is the continuous field of traction vectors defined at any spatial position (x,y) within the contact region.

RESULTS

Spatiotemporal distribution of neutrophil traction stresses during chemokinesis and chemotaxis

To determine how traction force asymmetry develops in response to different chemotactic gradients and how it might change over time, time-lapse measurements were performed on neutrophils migrating on stiff gels (12 kPa) for a range of fMLP gradients. Each column in Fig. 2 illustrates the spatial pattern of traction stress in a cell at a given time for three distinct gradients ($\Delta c/\Delta x = 0$, $C_M = 10$ nM; $\Delta c/\Delta x = 0.5$ nM/10 μm, $C_M = 10$ nM; and $\Delta c/\Delta x = 10$ nM/10 μm, $C_M = 100$ nM), and the arrow originating at the cell center indicates the direction and displacement of cell motion during the next minute after the image was taken. As shown in Fig. 2 *a*, chemokinetic neutrophils stimulated with a uniform solution of fMLP ($\Delta c/\Delta x = 0$, $C_M = 10$ nM) near the receptor K_D (~10 nM) orient their forces randomly. Although the highest traction forces are

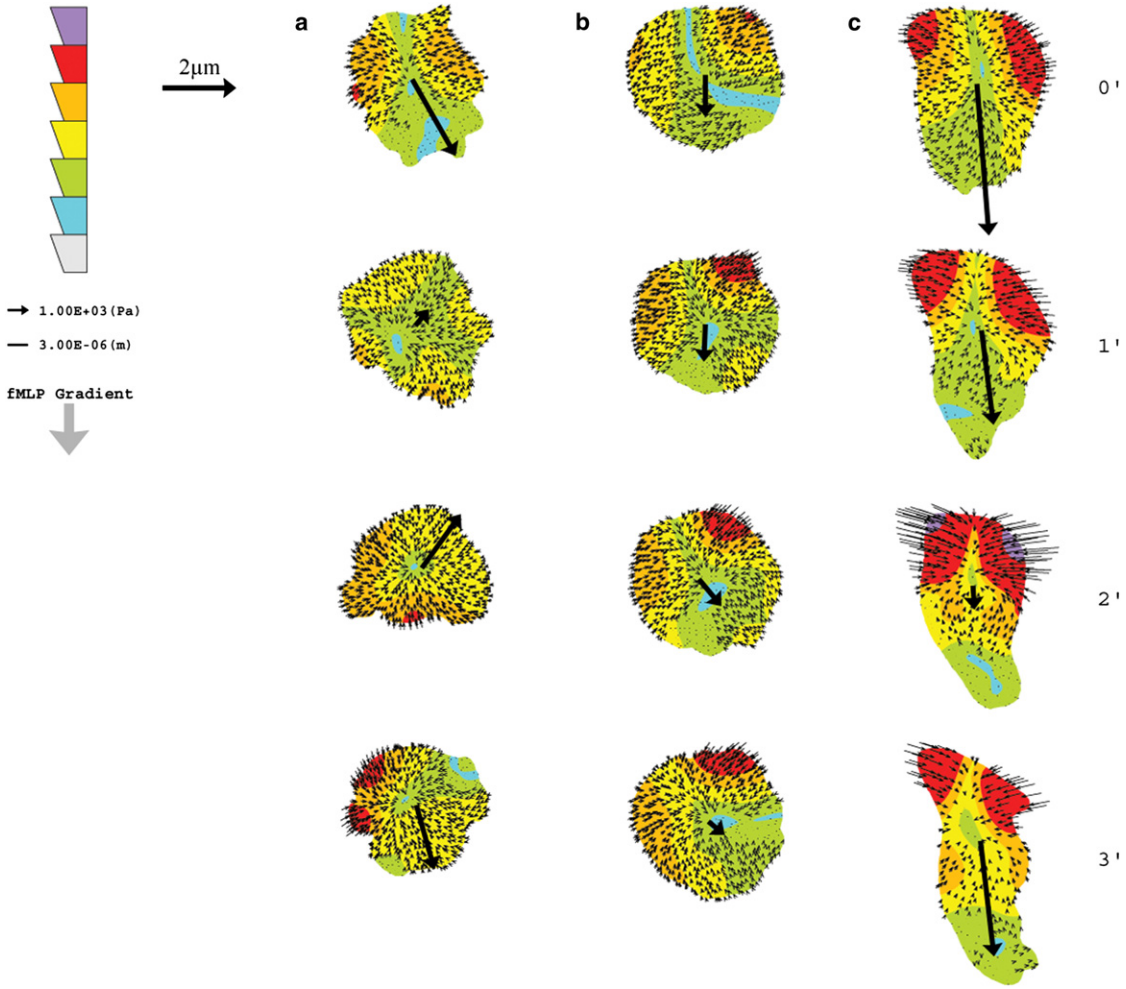

FIGURE 2 Spatial and temporal distribution of neutrophil traction stresses on a stiff hydrogel in response to varying fMLP gradients. (*a–c*) Neutrophil traction stress maps on stiff hydrogels (12 kPa) in response to a uniform solution of fMLP ($\Delta c/\Delta x = 0$, $C_M = 10$ nM) (*a*), a shallow gradient of fMLP ($\Delta c/\Delta x = 0.5$ nM/10 μm, $C_M = 10$ nM) (*b*), and a steep gradient of fMLP ($\Delta c/\Delta x = 10$ nM/10 μm, $C_M = 100$ nM) (*c*). The cell diameter of a neutrophil was assumed to be ~10 μm. Traction stress maps were collected at 1-min intervals. Large arrows drawn from the center of each cell indicate the direction of motility in the next time frame, and the length of the arrow corresponds to the magnitude of displacement. The direction of increasing fMLP concentration within the gradient in *b* and *c* is indicated by the downward arrow at the left. The color-scale bar at the left indicates the magnitude of traction stress, with the highest magnitude of stress at the top of the scale bar. Smaller arrows within each cell show the direction and magnitude of force vectors.

frequently oriented at the rear of the cell relative to the direction of migration, the direction of cell motility, and hence the orientation of forces, is random. Furthermore, the distribution of forces alternates between asymmetric and isotropic, such that the forces appear to reposition themselves randomly around the cell periphery. The results show that even in the absence of an external chemotactic gradient, a neutrophil can generate an asymmetric distribution of traction forces on a stiff 12-kPa hydrogel. When cells are placed in a shallow gradient of fMLP ($\Delta c/\Delta x = 0.5$ nM/10 μm, $C_M = 10$ nM) on stiff gels (12 kPa), traction force asymmetry is observed and forces are concentrated at the end of the cell located at the lower end of the fMLP gradient over a longer period of time (Fig. 2 *b*). In the presence of a steep chemotactic gradient ($\Delta c/\Delta x = 10$ nM/10 μm, $C_M = 100$ nM), neutrophil traction stress maps show that forces are higher in magnitude and are more strongly concentrated in the uropod of cells oriented in the fMLP gradient (Fig. 2 *c*). Root-mean-squared traction forces in the presence of a strong chemotactic gradient are maintained over time and are higher than forces observed during chemokinesis over several time-lapse measurements for stiff hydrogels (Fig. 3 *a*). These results suggest that external chemotactic gradients can influence the magnitude and distribution of traction forces on stiff hydrogels.

To determine how changes in substrate mechanics might influence traction stress distributions during chemokinesis and chemotaxis, time-lapse measurements were performed with neutrophils migrating on soft hydrogels (2 kPa). As shown in Fig. 4 *a*, traction stresses for neutrophils on soft hydrogels in a uniform solution of fMLP ($\Delta c/\Delta x = 0$,

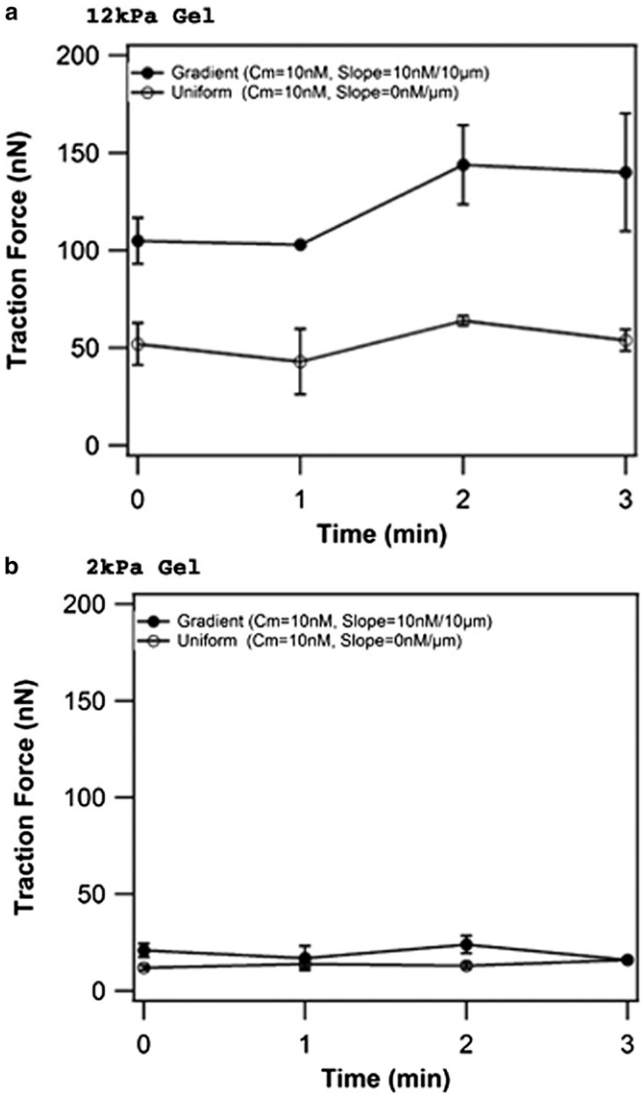

FIGURE 3 Magnitude of neutrophil traction force on a stiff and a soft hydrogel in response to uniform and gradient solutions of fMLP as a function of time. Traction forces for neutrophils migrating on (*a*) stiff (12 kPa) and (*b*) soft (2 kPa) hydrogels were measured at 1-min intervals and plotted as a function of time. A uniform fMLP solution with a mean concentration of 10 nM or a gradient solution with a mean concentration of 10 nM and slope of 10 nM/10 μm was applied to each gel stiffness. n = 2 cells at each time-point. Error bars represent one standard error.

C_M = 10 nM) are distributed isotropically. A few small regions of high stress are observed, but they are not consistently positioned at the rear of the cell relative to motion. This is in contrast to results obtained for neutrophils on stiff substrates after uniform stimulation (Fig. 2 *a*), where asymmetric distributions of traction stress develop stochastically and are often located in the uropod. In the presence of a steep chemotactic gradient ($\Delta c/\Delta x$ = 10 nM/10 μm, C_M = 100 nM) on a soft hydrogel, traction stress asymmetry develops over time (Fig. 4 *b*); however, the asymmetry and intensity of stresses is significantly lower than that observed for neutrophils on stiff hydrogels (Fig. 2 *c*). On soft hydrogels, the root-mean-squared forces under chemotaxis are not significantly different from those under chemokinesis (Fig. 3 *b*). These results suggest that asymmetric distributions of traction stress are influenced by substrate mechanics. Specifically, stiff hydrogel substrates appear to provide stronger cues for the organization of neutrophil force polarity in both the presence and absence of external chemical gradients.

Neutrophil traction forces and chemotactic index as a function of mean chemoattractant concentration and gradient steepness

To investigate how chemoattractant signals, chemotactic index, and traction forces are related, forces of neutrophils stimulated with different mean fMLP concentrations and gradient slopes were determined. Observations of neutrophils were made in four different regions of a microfluidic chemotaxis chamber with either uniform concentrations of fMLP or linear gradients. For each region of the chamber where measurements were made, a mean time-averaged concentration of fMLP (C_M) was calculated by averaging the expected low and high concentration of the gradient across that region. In a similar way, the slope of a region was determined by dividing the mean concentration by the length of the region ($\Delta c/\Delta x$). Since linear gradients were used, the slope remained constant across all regions of the chamber for a given chemoattractant condition. For neutrophils on 12-kPa hydrogels, traction forces do not change significantly in response to changes in mean fMLP concentration between 7 and 49 nM, when the gradient is held constant at 0.5 nM/10 μm and when the fMLP concentration is above the receptor K_D (~10 nM for fMLP) (Fig. 5 *a*) (33,34). As mean fMLP concentration is increased beyond the receptor K_D for a gradient of $\Delta c/\Delta x$ = 0.5 nM/10 μm, the chemotactic index decreases. Fig. 5 *b* illustrates how traction forces and directional motion, as quantified by the chemotactic index, are correlated on stiff materials and ideal chemotactic gradients where C_M is near the K_D or when the magnitude of the chemoattractant gradient is large. The lowest traction force of 50 nN is found in chemokinesis at $\Delta c/\Delta x = 0$ and C_M = 10 nM; this corresponds to random motion, as illustrated by a chemotactic index equal to zero. The highest force, ~90 nN, is displayed by cells in a strong gradient field, $\Delta c/\Delta x$ = 10 nM/10 μm and C_M = 10 nM; correspondingly, the chemotactic index is high (~0.7). The magnitude of the traction stress can then be decreased by either decreasing the magnitude of the chemoattractant gradient (to $\Delta c/\Delta x$ = 0.5 nM/10 μm at constant C_M = 10 nM) or increasing C_M to 100 nM at constant gradient. Again, the increase in C_M to $10K_D$ means a given gradient will be less effective at generating differential receptor occupancy. The decrease in traction stress correlates to a

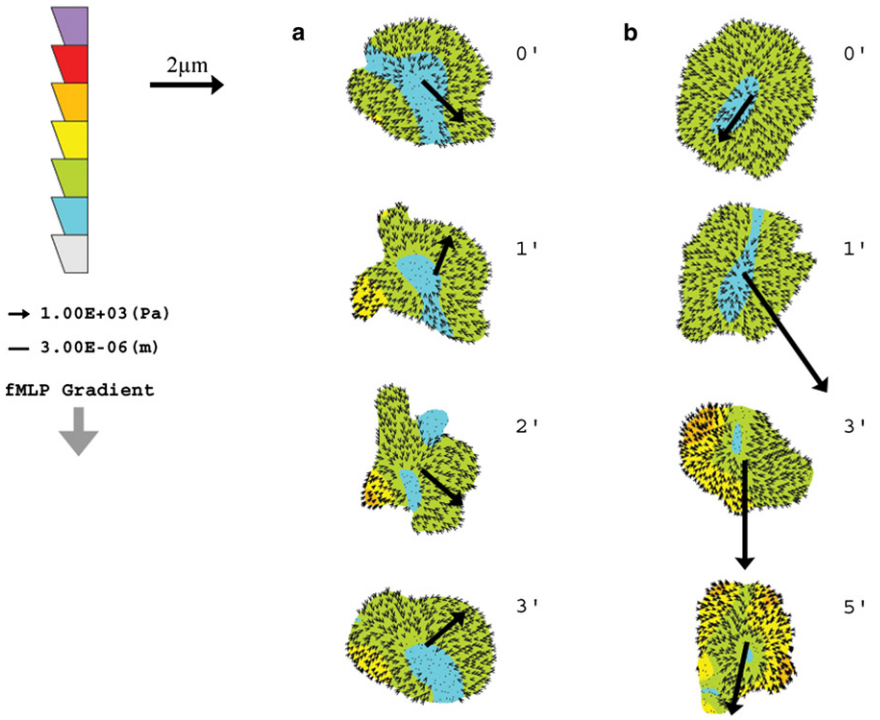

FIGURE 4 Spatial and temporal distribution of neutrophil traction stresses on a soft hydrogel in response to varying fMLP gradients. (*a* and *b*) Neutrophil traction stress maps on soft hydrogels (2 kPa) in response to a uniform solution of fMLP ($\Delta c/\Delta x = 0$, $C_M = 10$ nM) (*a*) and a steep gradient of fMLP ($\Delta c/\Delta x = 10$ nM/10 μm, $C_M = 100$ nM) (*b*). The cell diameter of a neutrophil was assumed to be ~10 μm. Traction stress maps were collected at 1- or 2-min intervals as indicated. Large arrows drawn from the center of each cell indicate the direction of motility in the next time frame, and the length of the arrow corresponds to the magnitude of displacement. The direction of increasing fMLP concentration within the gradient in *b* is indicated by the downward arrow at the left. The color scale bar at the left indicates the magnitude of traction stress, with the highest magnitude of stress at the top. Smaller arrows within each cell show the direction and magnitude of force vectors.

decrease in the chemotactic index. These results suggest that the magnitude of traction force and chemotactic index are responsive to changes in gradient steepness on stiff gels.

To determine whether similar responses to chemotactic signals are observed on soft hydrogels, neutrophil traction forces and chemotactic indexes for a range of mean concentrations and gradient slopes were measured on 2-kPa hydrogels (Fig. 5 *c*). The results show that neutrophil traction forces are not as responsive to changes in gradient steepness on soft hydrogels as they are on stiff hydrogels. As expected, the highest chemotactic index for neutrophils on soft gels is observed at a mean concentration of 10 nM and slope of 10 nM/10 μm. For a constant mean concentration of 10 nM, the chemotactic index increases with increasing gradient up to $\Delta c/\Delta x = 10$ nM/10 μm. It is interesting that for this gradient, the chemotactic index on a soft (2-kPa) gel approaches the chemotactic index seen on a stiff gel (Fig. 5 *b*) of 12 kPa under the same chemotactic gradient, without the generation of strong forces. At a mean concentration of 100 nM and gradient of 10 nM/10 μm, the chemotactic index decreases sharply and is lower than that observed for the same gradient on a stiff gel (Fig. 5, *b* and *c*). In addition, neutrophils on soft gels show a reduced chemotactic index in comparison to cells on stiff gels when the gradient is reduced to $\Delta c/\Delta x = 0.5$ nM/10 μm and $C_M = 10$ nM. Thus, measurement of force and directional motion on soft materials show that force and chemotaxis are not significantly correlated.

Integrin requirements during traction force generation

Previous work has shown that migration and traction forces are mediated by integrin receptors, but other, more recent work has shown that dendritic cells and T-cells show integrin-independent motility (27,35,36). β_2 integrins are the primary adhesion receptors in neutrophils and other leukocytes, and the hydrogels used in this study were functionalized with the β_2 integrin cognate ligand, ICAM-1. To further explore the molecular basis of force generation and observations of force asymmetry, and to determine to what extent neutrophils exert traction forces through integrins, we used TS1/18 antibody to block β_2 integrin receptors on neutrophils and subsequently stimulated these cells with fMLP gradients ($\Delta c/\Delta x = 10$ nM/10 μm, $C_M = 100$ nM) on both soft and stiff hydrogels. As shown in Fig. 6 *a*, blocking β_2 integrin receptors on neutrophils migrating on stiff gels leads to a significant decrease, but not an elimination, of traction force. In contrast, blocking β_2 integrin receptors on soft gels does not lead to a significant change in traction force, although these forces were already lower than on stiff gels. In addition to measuring changes in the average magnitude of traction force, we also examined the spatial distribution of traction stress. We find that addition of a β_2 blocking antibody removes the asymmetric distribution of forces typically observed on stiff hydrogels in the presence of a steep fMLP gradient (Fig. 6 *b*). Forces in a neutrophil treated with β_2 integrin blocking antibody are no longer located at the rear of the cell relative to the external gradient.

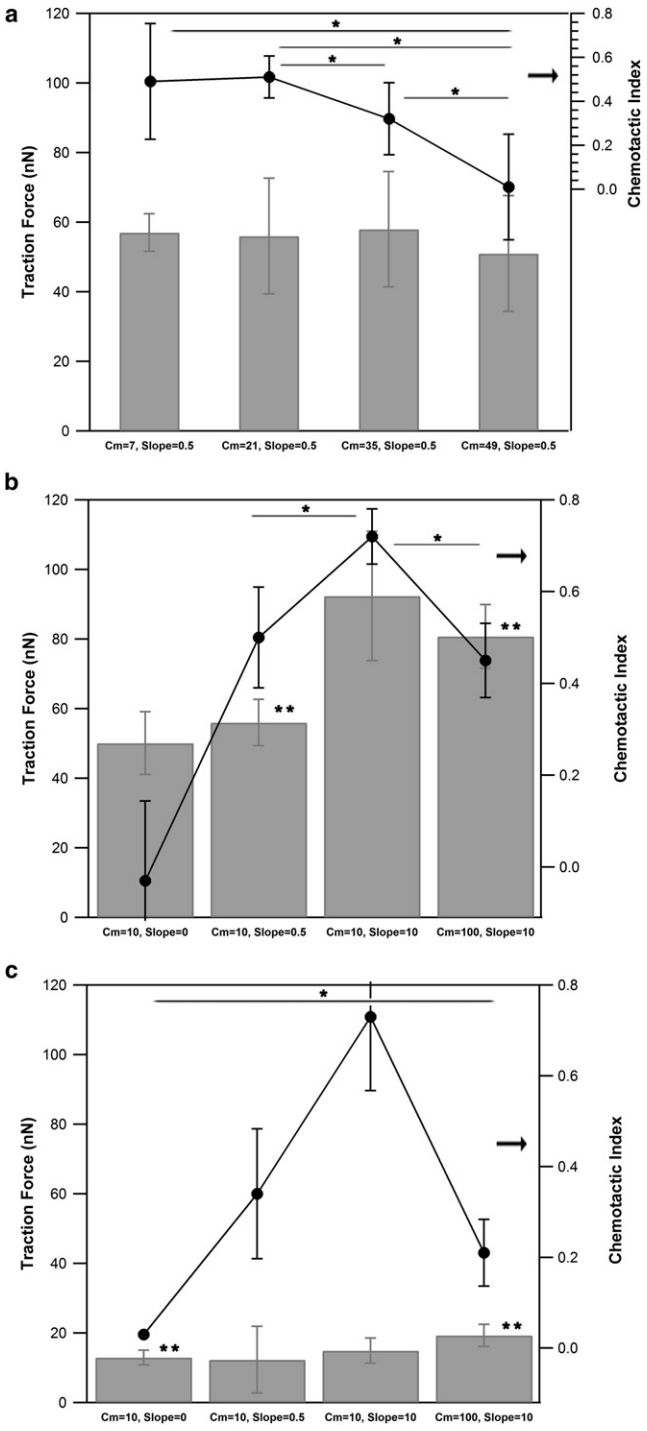

FIGURE 5 Traction force and chemotactic index of neutrophils in response to changes in mean fMLP concentration and gradient steepness. Average traction forces of neutrophils migrating in response to a range of mean fMLP concentrations and gradient slopes were measured and plotted with corresponding chemotactic indexes on stiff and soft hydrogels. (*a* and *b*) Measurements of neutrophils on a stiff gel (12 kPa) at varying mean fMLP concentrations and constant gradient of 0.5 nM/10 μm (*a*) and constant mean fMLP concentration and varying gradient slope (*b*). (*c*) Measurements of neutrophils on a soft gel (2 kPa) at constant mean fMLP concentration and varying gradient slope. Between 8 and 20 cells were measured for each chemotactic index value. Between 3 and 39 measurements were made for each traction force condition. Error bars represent 95% confidence intervals. *$P < 0.05$ for chemotaxis measurements; **$P < 0.05$ for traction force measurements.

However, it is interesting that there is some integrin-independent traction force in these cells. No significant change is observed in the map of traction stress for a neutrophil treated with integrin-blocking antibody on a soft gel, which remains largely unpolarized in its force distribution (Fig. 6 *c*). The data suggest that outside-in signaling through integrins contributes to neutrophil traction forces on stiff gels; however, integrin signaling does not contribute significantly to forces measured on soft hydrogels.

Effect of inhibiting RhoA and ROCK on traction-force generation

Integrin receptors are known to signal through RhoA in response to mechanical tension, and RhoA has been localized to the rear of live neutrophils during migration (25,26). RhoA signaling is also known to play a role in leukocyte chemoattractant activation (37). To test the hypothesis that RhoA is involved in force generation at the rear, we inhibited cellular contractility using the ROCK inhibitor Y-26732. ROCK is a downstream effector of RhoA that increases cell contractility through its interactions with myosin II. Here, we show that inhibition of RhoA signaling through ROCK leads to a decrease in traction forces of neutrophils on stiff hydrogels in the presence of an fMLP gradient with mean concentration of 100 nM and slope of 10 nM/10 μm (Fig. 6 *d*). Moreover, inhibition of ROCK signaling leads to a decrease in the asymmetric distribution of traction forces of neutrophils on stiff gels (Fig. 6 *e*). This suggests that the ability of a neutrophil to sense and respond to an external chemical gradient requires intracellular contractility and force generation through ROCK on stiff gels.

DISCUSSION

In this article, we have correlated chemical cues received through the fMLP chemotactic peptide receptor to the spatial organization of traction forces in human neutrophils by combining traction force microscopy with a microfluidic chamber to apply a linear chemoattractant field across the length of a cell. The relationship between chemotactic peptide receptor occupancy and directional motion in neutrophils is well known for cells crawling on rigid substrata (18,22). The directional motion of a neutrophil increases with an increasing gradient of chemoattractant peptide across the cell and is ideal when the mean concentration of chemoattractant at the cell's mid-body is equal to the K_D of ligand-receptor binding. We, and later others, showed previously that in response to chemotactic peptide

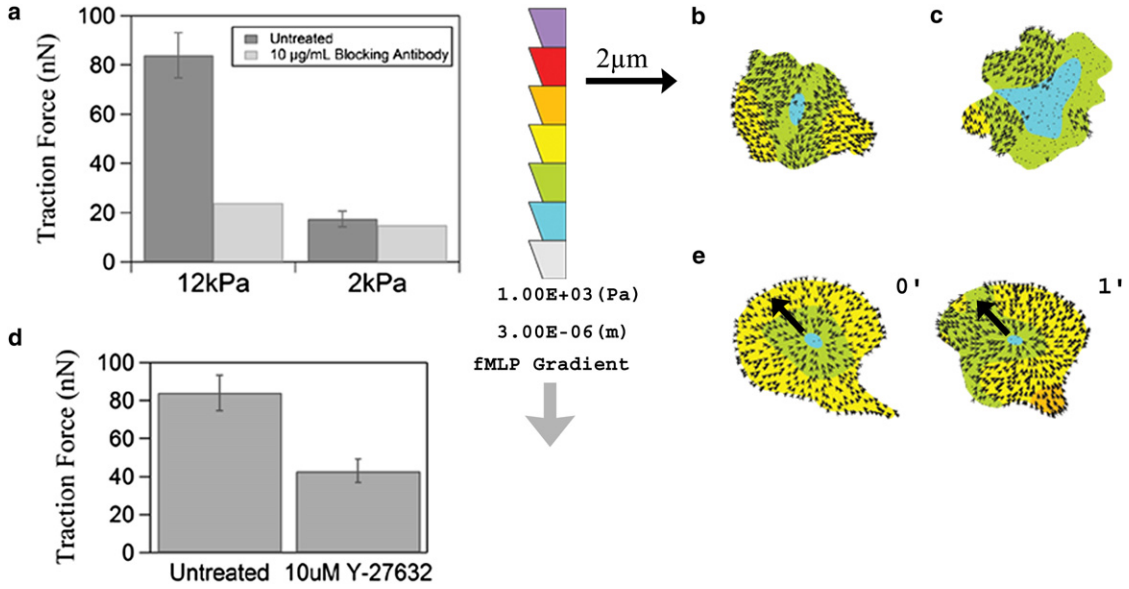

FIGURE 6 Neutrophil traction forces and stress maps in response to inhibition of integrin signaling. Neutrophils were incubated with 10 μg/mL TS1/18 β2 integrin blocking antibody before measurement of traction forces in the presence of an fMLP gradient with mean concentration of 100 nM and slope of 10 nM/10 μm. (*a*) Average traction forces of neutrophils treated with TS1/18 antibody on stiff or soft gels. n = 29–54 cells were measured for each untreated gel stiffness. (*b* and *c*) Traction stress maps of a neutrophil treated with TS1/18 antibody on a stiff gel (*b*) and a soft gel (*c*). (*d*) Neutrophils were incubated with 10 μM ROCK inhibitor before measurement of traction forces on stiff (12-kPa) hydrogels in response to an fMLP gradient with mean concentration of 100 nM and slope of 10 nM/10 μm (n = 54 cells measured for the untreated condition and 3 cells for the Y-27632 condition). (*e*) Representative traction stress maps of neutrophils treated with 10 μM ROCK inhibitor over a 1-min interval. The fMLP gradient in *b*, *c*, and *e* increases from top to bottom as illustrated by the downward arrow. The color scale bar in *b*, *c*, and *e* indicates the magnitude of traction stress within the cell boundary, with the highest magnitude of stress at the top. Error bars represent 95% confidence intervals.

exuded from a pipette, neutrophils concentrate traction stresses in the uropod (13,17). However, combining traction force microscopy with precise chemoattractant gradients might allow us to determine under what conditions traction stresses are correlated with differential receptor occupancy and directional motion, and under what conditions directional motion is independent of traction stress.

On stiffer gels of 12 kPa, we find that large peptide gradients or mean concentrations near the K_D lead to the formation of avid regions of contractile stress in the cell uropod and are accompanied by strong directed cell motion toward higher chemoattractant concentrations. Under these conditions of strong chemoattractant signaling, localized traction stresses are punctate and usually present in pairs, located in the uropod, and approach several kPa. When the chemoattractant signal is diminished, either by decreasing the magnitude of the gradient or increasing the mean chemoattractant concentration, the magnitude of the traction stresses lessens, although they remain punctate and often become asymmetric, and the cell moves less efficiently toward higher chemoattractant concentrations. When cells were placed in a uniform field of chemoattractant (chemokinesis), they moved randomly and displayed several weak centers of contractile stress that moved around the cell periphery.

The universal picture that emerges from this data is that the cell somehow responds to differential receptor occupancy by spatially organizing its contractile centers dorsal to the direction of chemoattractant signaling. An insight that may explain the spatial concentration of signaling motifs is the spatial coupling of stochastically driven signaling motifs around the cell periphery in response to receptor stimuli (38). The resulting motion stems from the squeezing of uropodial contractile centers that drive fluid toward the lamellipod. This conceptualization of leukocyte motion is consistent with a recently published model of spontaneous cell motion in keratinocytes and other cell types (39).

Previous work suggests that the spatial orientation of Rho GTPases such as Rac and RhoA are responsible for the spatial organization of a cell's internal machinery. Whereas active Rac is found in the leading edge, the Bourne laboratory used a FRET biosensor for RhoA to suggest that RhoA GTPase is the uropodial restricted enzyme that is responsible for directional motion (25). However, a direct link between RhoA activity, directional motion, and traction-force generation has never been made, to our knowledge. Here, using pharmacological inhibition of RhoA GTPase under conditions of avid chemotaxis, we clearly show that specifically inhibiting ROCK, the downstream target of RhoA, inhibits uropodial contractility and reduces traction stresses. We also observed that these cells displayed limited motility and did not translocate significant distances, and therefore we could not calculate a chemotactic index under these conditions. In the two cases where displacements are

illustrated (Fig. 5 *e*), displacements are smaller than the cell size and not aligned with the chemotactic gradient; in other cases, cells do not translocate at all. Our observations of the reduction of traction stresses and the failure of cells to translocate chemotactically are consistent with the theory that RhoA and its downstream target ROCK are important for the spatial organization of traction stresses and directional motion.

An interesting additional finding from this study is the role that cell-substrate mechanics and adhesion play in supporting directional migration. In these experiments, we focused on the adhesion ligand ICAM-1. This physiologically relevant ligand binds to β_2-integrin receptors, and one can think of the experiments here as an idealization of neutrophil motion over the endothelial apical surfaces. Further, previous work on mapping contractile stresses involved ICAM-1 surfaces (13), so this substrate provides meaningful comparisons. We found that when cells were motile on stiffer gels (12 kPa), inhibiting chemotaxis using an antibody against β_2-integrin led to a decrease, but not an elimination, of traction stresses and directional motion. Further, the uropodial traction stresses were largely eliminated, but some vestigial lamellipodial stresses remained. This result agrees with that seen by Sixt and co-workers, who showed that immune cells can enter tissues without the use of integrins (35). We also were interested to find that on soft gels (2 kPa), although cell organization and the ability to exert traction stress were greatly reduced, the motility that remained was largely integrin-independent. These results lead to two striking conclusions. First, neutrophils possess multiple mechanisms of motility, with redundant, overlapping functions; and second, substrate stiffness, which has been shown to modulate cell function (26), may be doing so through its ability to organize integrin receptors and their attendant downstream activation. Soft gels may prevent receptor organization and leave cells to employ only integrin-independent mechanisms of motion.

Given the tools presented herein, our future goals are to test the universality of the principles we have found here across other amoeboid cells and, further, to perform intracellular molecular manipulations that allow us to understand how intercellular components may be responsible for coupling chemotactic signaling to the spatiotemporal control of traction stress and ultimately directed cell motility.

This work was supported by National Institutes of Health Grant HL18208 and a fellowship from Merck (to R.A.J.).

REFERENCES

1. du Roure, O., A. Saez, …, B. Ladoux. 2005. Force mapping in epithelial cell migration. *Proc. Natl. Acad. Sci. USA.* 102:2390–2395.
2. Munevar, S., Y. L. Wang, and M. Dembo. 2001. Distinct roles of frontal and rear cell-substrate adhesions in fibroblast migration. *Mol. Biol. Cell.* 12:3947–3954.
3. Beningo, K. A., K. Hamao, …, H. Hosoya. 2006. Traction forces of fibroblasts are regulated by the Rho-dependent kinase but not by the myosin light chain kinase. *Arch. Biochem. Biophys.* 456:224–231.
4. Tan, J. L., J. Tien, …, C. S. Chen. 2003. Cells lying on a bed of microneedles: an approach to isolate mechanical force. *Proc. Natl. Acad. Sci. USA.* 100:1484–1489.
5. Reinhart-King, C. A., M. Dembo, and D. A. Hammer. 2003. Endothelial cell traction forces on RGD-derivatized polyacrylamide substrata. *Langmuir.* 19:1573–1579.
6. Lo, C. M., H. B. Wang, …, Y. L. Wang. 2000. Cell movement is guided by the rigidity of the substrate. *Biophys. J.* 79:144–152.
7. Harris, A. K., P. Wild, and D. Stopak. 1980. Silicone rubber substrata: a new wrinkle in the study of cell locomotion. *Science.* 208:177–179.
8. Balaban, N. Q., U. S. Schwarz, …, B. Geiger. 2001. Force and focal adhesion assembly: a close relationship studied using elastic micropatterned substrates. *Nat. Cell Biol.* 3:466–472.
9. Beningo, K. A., M. Dembo, …, Y. L. Wang. 2001. Nascent focal adhesions are responsible for the generation of strong propulsive forces in migrating fibroblasts. *J. Cell Biol.* 153:881–888.
10. Galbraith, C. G., and M. P. Sheetz. 1999. Keratocytes pull with similar forces on their dorsal and ventral surfaces. *J. Cell Biol.* 147:1313–1324.
11. Lee, J., M. Leonard, …, K. Jacobson. 1994. Traction forces generated by locomoting keratocytes. *J. Cell Biol.* 127:1957–1964.
12. Lombardi, M. L., D. A. Knecht, …, J. Lee. 2007. Traction force microscopy in *Dictyostelium* reveals distinct roles for myosin II motor and actin-crosslinking activity in polarized cell movement. *J. Cell Sci.* 120:1624–1634.
13. Smith, L. A., H. Aranda-Espinoza, …, D. A. Hammer. 2007. Neutrophil traction stresses are concentrated in the uropod during migration. *Biophys. J.* 92:L58–L60.
14. Iwadate, Y., and S. Yumura. 2008. Actin-based propulsive forces and myosin-II-based contractile forces in migrating *Dictyostelium* cells. *J. Cell Sci.* 121:1314–1324.
15. Ambrosi, D., A. Duperray, …, C. Verdier. 2009. Traction patterns of tumor cells. *J. Math. Biol.* 58:163–181.
16. Jannat, R. A., G. P. Robbins, …, D. A. Hammer. 2010. Neutrophil adhesion and chemotaxis depend on substrate mechanics. *J. Phys. Condens. Matter.* 22:194117.
17. Oakes, P. W., D. C. Patel, …, J. X. Tang. 2009. Neutrophil morphology and migration are affected by substrate elasticity. *Blood.* 114:1387–1395.
18. Lauffenburger, D. A., and J. J. Linderman. 1993. Receptors: Models for Binding, Trafficking, and Signaling. Oxford University Press, New York.
19. Devreotes, P. N., and S. H. Zigmond. 1988. Chemotaxis in eukaryotic cells: a focus on leukocytes and *Dictyostelium*. *Annu. Rev. Cell Biol.* 4:649–686.
20. Zigmond, S. H. 1977. Ability of polymorphonuclear leukocytes to orient in gradients of chemotactic factors. *J. Cell Biol.* 75:606–616.
21. Reference deleted in proof.
22. Zigmond, S. H. 1977. Ability of polymorphonuclear leukocytes to orient in gradients of chemotactic factors. *J. Cell Biol.* 75:606–616.
23. Tranquillo, R. T., D. A. Lauffenburger, and S. H. Zigmond. 1988. A stochastic model for leukocyte random motility and chemotaxis based on receptor binding fluctuations. *J. Cell Biol.* 106:303–309.
24. Xu, J., F. Wang, …, H. R. Bourne. 2003. Divergent signals and cytoskeletal assemblies regulate self-organizing polarity in neutrophils. *Cell.* 114:201–214.
25. Wong, K., O. Pertz, …, H. Bourne. 2006. Neutrophil polarization: spatiotemporal dynamics of RhoA activity support a self-organizing mechanism. *Proc. Natl. Acad. Sci. USA.* 103:3639–3644.
26. Paszek, M. J., N. Zahir, …, V. M. Weaver. 2005. Tensional homeostasis and the malignant phenotype. *Cancer Cell.* 8:241–254.
27. Woolf, E., I. Grigorova, …, R. Alon. 2007. Lymph node chemokines promote sustained T lymphocyte motility without triggering stable integrin adhesiveness in the absence of shear forces. *Nat. Immunol.* 8:1076–1085.

28. Pelham, Jr., R. J., and Y. L. Wang. 1997. Cell locomotion and focal adhesions are regulated by substrate flexibility. *Proc. Natl. Acad. Sci. USA.* 94:13661–13665.

29. Pless, D. D., Y. C. Lee, …, R. L. Schnaar. 1983. Specific cell adhesion to immobilized glycoproteins demonstrated using new reagents for protein and glycoprotein immobilization. *J. Biol. Chem.* 258:2340–2349.

30. Dertinger, S. K. W., D. T. Chiu, …, G. M. Whitesides. 2001. Generation of gradients having complex shapes using microfluidic networks. *Anal. Chem.* 73:1240–1246.

31. Li Jeon, N., H. Baskaran, …, M. Toner. 2002. Neutrophil chemotaxis in linear and complex gradients of interleukin-8 formed in a microfabricated device. *Nat. Biotechnol.* 20:826–830.

32. Dembo, M., and Y. L. Wang. 1999. Stresses at the cell-to-substrate interface during locomotion of fibroblasts. *Biophys. J.* 76:2307–2316.

33. Herzmark, P., K. Campbell, …, H. R. Bourne. 2007. Bound attractant at the leading vs. the trailing edge determines chemotactic prowess. *Proc. Natl. Acad. Sci. USA.* 104:13349–13354.

34. Sullivan, S. J., G. Daukas, and S. H. Zigmond. 1984. Asymmetric distribution of the chemotactic peptide receptor on polymorphonuclear leukocytes. *J. Cell Biol.* 99:1461–1467.

35. Lämmermann, T., B. L. Bader, …, M. Sixt. 2008. Rapid leukocyte migration by integrin-independent flowing and squeezing. *Nature.* 453: 51–55.

36. Choquet, D., D. P. Felsenfeld, and M. P. Sheetz. 1997. Extracellular matrix rigidity causes strengthening of integrin-cytoskeleton linkages. *Cell.* 88:39–48.

37. Laudanna, C., J. J. Campbell, and E. C. Butcher. 1996. Role of Rho in chemoattractant-activated leukocyte adhesion through integrins. *Science.* 271:981–983.

38. Weiger, M. C., S. Ahmed, …, J. M. Haugh. 2010. Directional persistence of cell migration coincides with stability of asymmetric intracellular signaling. *Biophys. J.* 98:67–75.

39. Herant, M., and M. Dembo. 2010. Form and function in cell motility: from fibroblasts to keratocytes. *Biophys. J.* 98:1408–1417.